IEEE Access
Multidisciplinary ⋮ Rapid Review ⋮ Open Access Journal

Received 6 January 2023, accepted 5 March 2023, date of publication 14 March 2023, date of current version 17 March 2023.

*Digital Object Identifier 10.1109/ACCESS.2023.3257050*

RESEARCH ARTICLE

# Folded-Dipole Antenna Geometrical Analysis for THz Microbolometer

**ARIE PANGESTI AJI[1,3], HIROAKI SATOH[2], (Member, IEEE), CATUR APRIONO[3], (Member, IEEE), EKO TJIPTO RAHARDJO[3], (Member, IEEE), AND HIROSHI INOKAWA[2], (Member, IEEE)**

[1]Graduate School of Science and Technology, Shizuoka University, Hamamatsu 432-8011, Japan
[2]Research Institute of Electronics, Shizuoka University, Hamamatsu 432-8011, Japan
[3]Department of Electrical Engineering, Universitas Indonesia, Depok 16424, Indonesia

Corresponding author: Hiroshi Inokawa (inokawa.hiroshi@shizuoka.ac.jp)

This work was supported in part by the Cooperative Research Project of the Research Center for Biomedical Engineering with the Research Institute of Electronics (RIE), Shizuoka University; and in part by the Cooperative Research Project Program of Research Institute of Electrical Communication (RIEC), Tohoku University.

**ABSTRACT** To improve the responsivity of terahertz (THz) antenna-coupled bolometer, heater (load) resistance has to be increased to suppress the thermal conduction and realize larger temperature rise of the thermistor. Proper design of antenna is therefore essential to assure the impedance matching between antenna and heater. From this viewpoint, a high-impedance folded-dipole antenna (FDA) has been studied numerically by the finite element simulation. The effect of FDA structural parameters such as number of arms, antenna width, and arm spacing are discussed with the lumped port and resistive heater coupled to the antenna gap for the cases of radiating and receiving modes, respectively. The product of resonant resistance and area efficiency is used to predict the improvement made by FDA as a figure of merit (FOM) correlated to the bolometer responsivity. This study revealed that the optimum FOM in FDA-coupled bolometer operating at 1 THz was obtained with three arms, 1-$\mu$m antenna width and 4-$\mu$m arm spacing. A comparison was made with the result from a half-wave dipole antenna and revealed that FDA could enhance the bolometer responsivity by a factor of 15. This research demonstrated the effectiveness of the FDA to improve the performance of THz antenna-coupled bolometer for applications such as imaging for non-destructive inspection.

**INDEX TERMS** Terahertz, folded-dipole antenna, bolometer, heater, impedance matching, area efficiency.

## I. INTRODUCTION

Terahertz (THz) waves (0.1-30 THz) are perceived as valuable mainly due to the unique spectral absorption by middle and high molecule substances, good transparency for non-polar materials, high reflection by metals, and negligible radiation damage to living tissue under inspection [1], [2]. As a result, various THz applications have been proposed in recent decades, such as medical diagnosis [3], non-destructive inspection [4] and astronomical observations [5] as well as high-speed wireless communication [6]. The wide range of THz applications are generally supported by the semiconductor detectors based on mechanisms such as non-linear response of Schottky diode and FET, and photo-generation of carriers in quantum wells (QW) and dots (QD). Another detection mechanism is the thermal sensing which is advantageous in terms of the room-temperature operation, simple device structure and the coverage of wide wavelength range. Hence it is perceived that the thermal detector is a better option for THz image sensor operating at room temperature [7].

Bolometer as one kind of thermal detectors, senses the resistance change of semiconducting or metallic film caused by the temperature rise associated with the absorption of incident THz radiation. The sensitivity of a bolometer is largely affected by the thermal conduction to the supporting structures such as substrate and the surrounding environment. For that reason, it is crucial to design a bolometer with a low thermal conduction by suspended structure with long and narrow supporting legs. However, as wavelength becomes

The associate editor coordinating the review of this manuscript and approving it for publication was Wanchen Yang.

longer in the THz region, such thermal isolation is mechanically difficult. Therefore, antenna-coupled microbolometer becomes a viable solution in which only the part consisting of heater and thermistor is thermally isolated above the cavity. The incident electromagnetic wave is received by the antenna, and the energy is transferred to the coupled heater to raise the temperature. Furthermore, the induced Joule heat is converted into electrical signal by the resistive temperature sensor (thermistor) [8].

Responsivity and noise equivalent power (NEP) are the two main parameters in analyzing the bolometer performance, which are the ratio of the voltage output to the input power and the smallest measurable power by the bolometer, respectively [9]. Recent studies on the scaling of antenna-coupled bolometer suggested the importance of higher heater resistance to improve the responsivity and NEP simultaneously [10]. Consequently, a high-impedance antenna is necessary for proper impedance matching between antenna and heater. Folded dipole antennas (FDAs) having constructed from a standard half-wave dipole antenna with longer effective length is one of the feasible solutions. In FDA, the radiating part is miniaturized to form a meander structure. Furthermore, it can be implemented as a planar structure and optimized based on its geometrical arrangements [11]. FDA has been extensively studied for the micro-nano optics as well as THz applications. A 2.75 kΩ FDA on GaAs substrate has been reported to enhance photomixer output power at 396 GHz compared to a broadband antenna [12]. Heterostructure backward tunnel diode (HBD) detector has been integrated with FDA monolithically to optimize the impedance matching thus improve its sensitivity [13]. A 6-dB power improvement by FDA compared to a log-periodic antenna has also been reported for CW THz photomixer [14]. The studies of FDA pointed out the importance of the antenna parametric study for the optimum design related to the impedance matching and efficiency.

Although the implementation of FDA can substantially improve the performance of THz sources and detectors, one should notice that the antenna efficiency is deteriorated due to the presence of high ohmic losses at the antenna surface [15]. However, the high resistance characteristics in the coupled heater is still advantageous for the overall bolometer performance. With the intention of optimal bolometer responsivity improvement, we propose a novel method to numerically investigate the THz FDA for optimized absorption of THz wave for bolometer application. The FDA input impedance and antenna area efficiency are investigated based on the structural parameters in the radiating and receiving modes, respectively. The improvement in responsivity is predicted by the figure of merit (FOM) which is the product of antenna area efficiency and heater resistance in an impedance matched condition. Furthermore, a comparison is made with the result of half-wave dipole antenna coupled to a low resistance heater. As the heater resistance can be adjusted by the downscaling to nanometer scale, the FDA is designed to attain high-resistance characteristics around 1 kΩ by the study on geometrical parameters such as number of arms, antenna width and arm spacing. The antenna designed on a high-resistivity silicon (Si) substrate allows one to consider the real FDA experiment in the presence of the substrate. The time domain solver of the CST Studio Suite software is used for the numerical computation.

## II. METHODOLOGY

The simulation model consists of a high-resistivity Si substrate, a vacuum airbox, and gold (Au) antenna, as illustrated in Fig. 1a. This model ensures the simulation domain include the high directivity performance through high resistivity substrate due to elimination of surface waves [16], [17]. The real physical thickness of the Si substrate is 525 $\mu$m with a refractive index of 3.42. Within this thickness, the substrate can be modeled to behave as a semi-infinite thick layer which is about 4 times larger than the effective wavelength at 1 THz. Therefore, we designed the wafer as a 20 $\mu$m thick Si box, backed by a perfectly matched layer (PML) boundary to form a semi-infinite substrate thickness. Time domain solver was used based on the finite integration technique (FIT) simulation in CST software. The model was discretized using hexahedral meshing combined with perfect boundary approximation (PBA) to improve the geometry description with efficient memory compared to the standard finite differential time domain (FDTD) method [18]. In the global hexahedral mesh properties, the mesh size was determined by a maximum 15 cells per wavelength. The perfectly matched layer (PML) absorbing boundary was defined in all the outer surfaces of the simulation model with the estimated reflection level of $10^{-4}$. As a result, the total number of $1.5 \times 10^6$ and $3.5 \times 10^6$ mesh cells were roughly generated. The computational time took around 10 minutes and 180 minutes for radiating and receiving mode simulations, respectively for the steady-state condition. The computational server was equipped with 3 GHz Intel Xeon E5-2687W based CPU and 128 GB of memory.

Fig. 1b shows the FDA structure consist of antenna length ($L_a$), width ($w_a$), arm spacing ($S$) and number of arms ($N$) equals to $2(k-1)+1$. The antenna gap ($g$) was set to be fixed at 11.5 $\mu$m wide. The antenna thickness was set to 200-nm, larger than the skin-depth of the antenna material at 1 THz frequency. A 50 Ω discrete port was used on the antenna gap as the source excitation for radiating mode simulation. In receiving mode simulation, a 1 V/m plane wave was triggered from the substrate side towards z+ direction. We consider this configuration because the antenna on a thick dielectric substrate radiates preferentially into the dielectric half space, thus higher directivity could be attained from the substrate side. The polarization and electric field vector of the plane wave were set to be linear and parallel to the x-axis of the antenna, respectively. A 50 nm thick titanium (Ti) heater slab was designed on the antenna gap to receive the induced displacement currents from the antenna, as illustrated in Fig. 1c and 1d. To keep the reciprocal input impedance

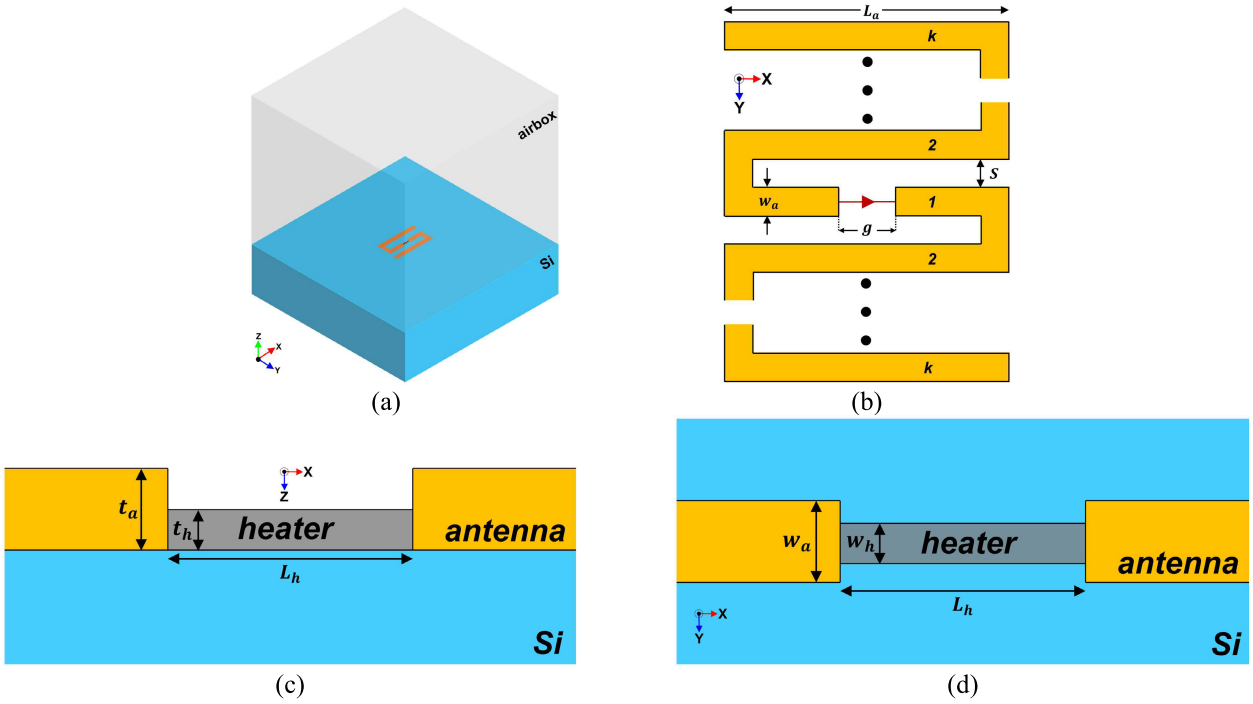


**FIGURE 1.** (a) Simulation model in 3D volumetric structure comprising of high resistivity Si substrate, a vacuum airbox, and antenna, (b) 2D FDA geometry parameters, (c) Cross sectional view of the Ti heater design, (d) Top view of the Ti heater design at the antenna gap.

behavior of the antenna in both radiating and receiving mode, the length of the heater was kept the same as the antenna gap size ($L_h = g$). Furthermore, the heater width ($w_h$) was set according to the electrical resistance equals to the resonant resistance ($R_r$) of the antenna in the radiating mode simulations, calculated as

$$w_h = \frac{\rho l_h}{R_r t_h} \tag{1}$$

where $\rho$, $L_h$, and $t_h$ are the resistivity, length, and thickness of the Ti heater, respectively. Within this heater design, the impedance matched condition between antenna and heater can be hypothesized. A power monitor was used in the receiving mode simulation to store the Poynting vectors of the electromagnetic field stimulated by the plane wave. Hence the power dissipation into lossy materials, such as Ti metal for the heater, can be extracted by the integration of Poynting vectors over the enclosed surfaces. The Au antenna and Ti heater were modeled with the electrical conductivity of $4.4 \times 10^7$ S/m and $2.6 \times 10^6$ S/m, respectively [19]. The effects of geometrical structure parameters of FDA on THz wave absorption of microbolometer structure, including antenna length ($L_a$), width ($w_a$), arm spacing ($S$) and number of arms ($N$) were studied by changing different structural parameters.

## III. SIMULATION RESULTS

### A. RADIATING MODE

Parametric study of the FDA was performed to analyze the effect of antenna geometries, such as length, width, and arm spacing to the input impedance characteristic. As the FDA resonant frequency depends mainly on its length, firstly we determine the resonant resistance ($R_r$) and resonant length ($L_r$) when the imaginary part of the input impedance ($Z_{in}$) crosses zero at the designated frequency of 1 THz. Fig. 2 illustrates the results for the case of three-arm FDA ($N = 3$) and fixing the antenna width ($w_a$) and arm spacing ($S$) to 1 $\mu$m and 4 $\mu$m, respectively. Fig. 2a shows the $Z_{in}$ of FDA extracted at 1 THz versus antenna length ($L_a$). The length is shown as the ratio to effective wavelength ($\lambda_s$) which is the wavelength at the interface between vacuum and Si substrate, calculated by

$$\lambda_s = \frac{\lambda_0}{\sqrt{\varepsilon_{eff}}} \tag{2}$$

where $\varepsilon_{eff}$ is the effective permittivity on the boundary of Si substrate ($\varepsilon = 11.7$) and free space ($\varepsilon = 1$), and $\lambda_0$ is the free space wavelength at 1 THz. It can be seen from Fig. 2a that the reactive component of the input impedance changes from inductive to capacitive behavior as $L_a$ increases. The resonant frequency obtained when $L_a = 0.512\ \lambda_s$, indicates that the $L_r$ of FDA is analogous to a classic half-wave dipole antenna. Fig. 2b shows the corresponding frequency response of the input impedance when the resonant length ($L_r$) equals to $0.512\ \lambda_s$. A maximum impedance of 675 Ω is extracted, which is much larger than the typical half-wave dipole impedance on a Si substrate.

The effect of $w_a$ and $S$ to the resonant length and input impedance are then investigated. The $R_r$ and $L_r$ were extracted from each $w_a$ and $S$ parameterization for the

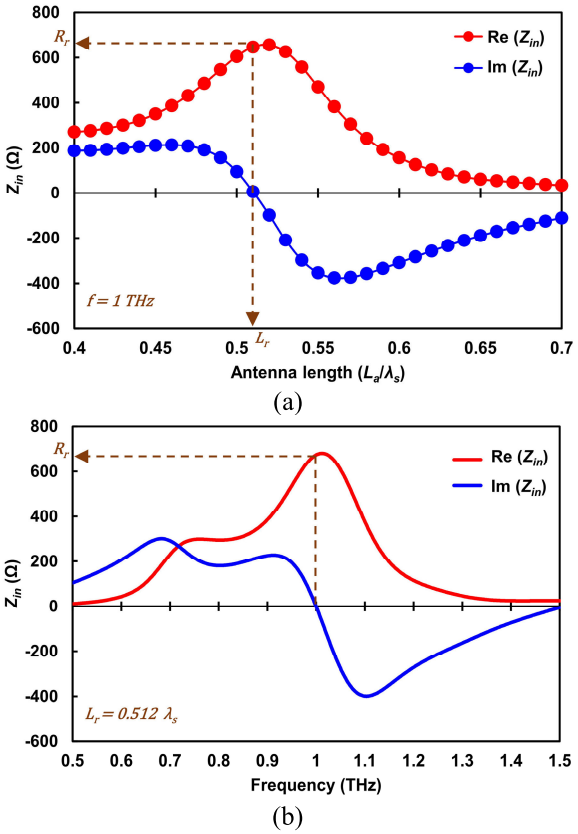


**FIGURE 2.** Input impedance ($Z_{in}$) characteristics of FDA for $N = 3$, $w_a = 1$ $\mu$m, and $S = 4$ $\mu$m: (a) Resonant resistance ($R_r$) and length ($L_r$) extraction from the point where the imaginary part crosses zero at 1 THz in various antenna length, (b) $Z_{in}$ of FDA resonates at 1 THz for $L_r = 0.512$ $\lambda_s$, $N = 3$, $w_a = 1$ $\mu$m, and $S = 4$ $\mu$m.

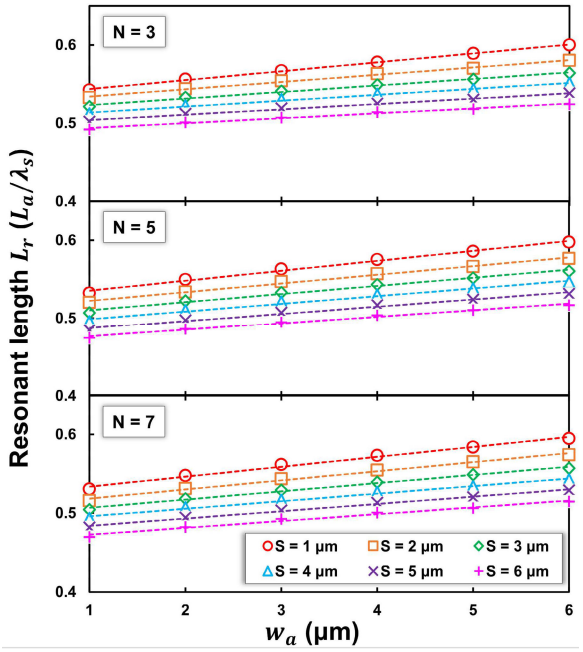


**FIGURE 3.** Resonant length ($L_r$) of FDA as a function of antenna width ($w_a$) in different arm spacing ($S$) and number of arms ($N$).

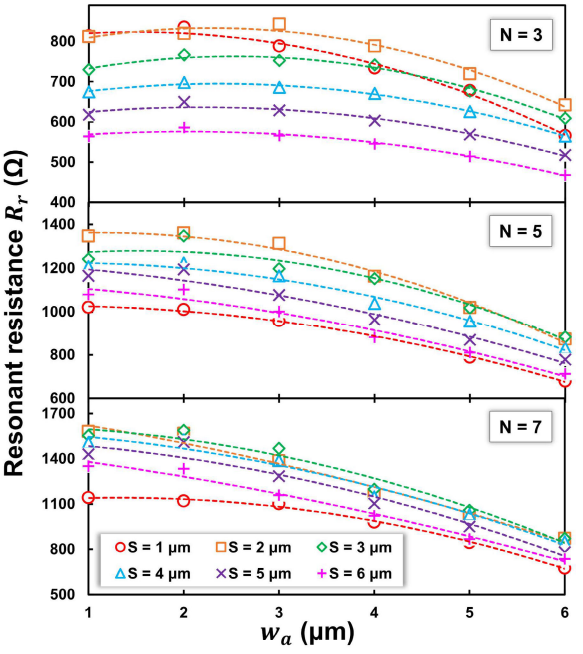


**FIGURE 4.** Resonant resistance ($R_r$) of FDA as a function of antenna width ($w_a$) in different arm spacing ($S$) and number of arms ($N$).

$N = 3$, 5 and 7. Fig. 3 shows the $L_r$ with respect to $w_a$ in different $S$ and $N$. The $L_r$ found around 0.5 $\lambda_s$ for all width and spacing variations which comparable to the resonant length of the classic half-wave dipole antenna. The $L_r$ shows opposite trend to the increase of $w_a$ and $S$, where it is linearly increase to the former and decrease to the latter. Yet this behavior is commonly different from the ordinary planar half-wave dipole antenna where the antenna length and width have opposite behavior to the resonant frequency. This could be explained by the fact that the resonant frequency of planar folded antenna is changing as a function of the width to the spacing ratio for a fixed length [11]. Accordingly, as we extract the results from a single frequency, it affected to the linear increase of the antenna resonant length to the antenna width but decrease to the arm spacing. In addition, the number of arms has a minor effect to the $L_r$ which implies the uniform half-wave resonant length behavior in FDA regardless the input impedance.

The corresponding resonant resistance ($R_r$) is then extracted from each resonant length ($L_r$), as shown in Fig. 4. The $R_r$ increase with the $N$ as longer effective length would yield higher resistance. The $R_r$ of three-arm FDA is ranging from 450 to 820 Ω in different $w_a$ and $S$. A slight increase of $R_r$ appeared when $w_a = 1{\sim}3$ $\mu$m and then decrease as $w_a$ increase further due to larger cross-sectional area of the antenna. As for $S = 1{\sim}2$ $\mu$m show resistance increase and further decrease as the S larger. From these variations, it suggests a saturated $R_r$ around the $w_a$ and $S$ of 2 $\mu$m. Slightly different behavior is found in FDA with $N = 5$ and 7, where the maximum $R_r$ exceeds 1.3 kΩ and

1.5 kΩ, respectively. As $N$ increases, the narrow spacing effect is stronger where very low $R_r$ obtained in the spacing of 1 $\mu$m when $N = 5$ and 7. However, the effect of w_a reduces where no peak $R_r$ found in the $w_a$ wider than 1 $\mu$m. These results give a trade-off behavior between $w_a$ and $S$ to the FDA resonant resistances in different $N$. The resistance decay in close proximity of FDA arms related to the strong mutual coupling which causes interchange of the energy. Some of the energy radiated from FDA arms were received by the other arms and then re-scattered in peculiar directions behaving as subsequent transmitters. In a very strong mutual coupling effect, the vector sum of radiated and re-scattered waves influences the input impedance in the antenna gap terminal and complicates the analysis. In a practical manner, mutual coupling between FDA arms is difficult to predict but must be considered due to its substantial contribution to the antenna impedance. Hence in this report we qualitatively predict the optimum proximity between FDA arms is 2 $\mu$m to obtain highest resistance with any number of arms. While in the narrow width case, the decaying resistance can be explained by the size effect caused from the mean free path of conduction electrons, which limits the electrical properties of a metal [20]. From the input impedance simulation results, it is concluded that a proper design process is critical when applying FDA to select desired resonant resistance for the impedance matching with the bolometer.

Furthermore, the radiation efficiency results are extracted, which explain the capability of the antenna to converts the RF power accepted from the source terminal into dielectric or free-space radiation. It can be described as the ratio of the radiated power to the total power delivered including conduction loss caused by the antenna material. Fig. 5 show the radiation efficiency of FDA as a function of resonant resistance ($R_r$) at 1 THz for different $N$. The radiation efficiency decreases as the $R_r$ increases ($w_a$ decreases) for any given arm spacing and number of arms. This phenomenon accounted for the higher conduction (ohmic) loss as an effect of the skin depth in high frequency where the electrical current is flowing on the conductor surface instead of the full cross-sectional area. Hence the conductive heating loss on the antenna surface increases as the cross-sectional area decreases. Since the actual $R_r$ comprises of radiation and loss resistance, the increase of ohmic loss affect to the reduction of radiation resistance, thus lower the radiation efficiency. Similar behavior occurs in all $S$ and $N$ variations. However, FDA with larger spacing shows higher radiation efficiency compared to closer one, even with the same $R_r$. The radiation efficiency has a large difference between 1 $\mu$m and 2 $\mu$m arm spacing, where the former is significantly lower. This suggests the importance of FDA arm spacing adjustment due to mutual coupling in between antenna arms that degrades the antenna efficiency. From radiation resistance and efficiency results in radiating mode, it is clear that there is a tradeoff between the two. Higher number of arms and narrow width is desirable for high resistance performance, but with the consequence of decreasing radiation efficiency. Nevertheless, larger arm spacing could be applied to increase the radiation efficiency but with the impact of the larger pixel size which may increase the complexity during nanofabrication process.

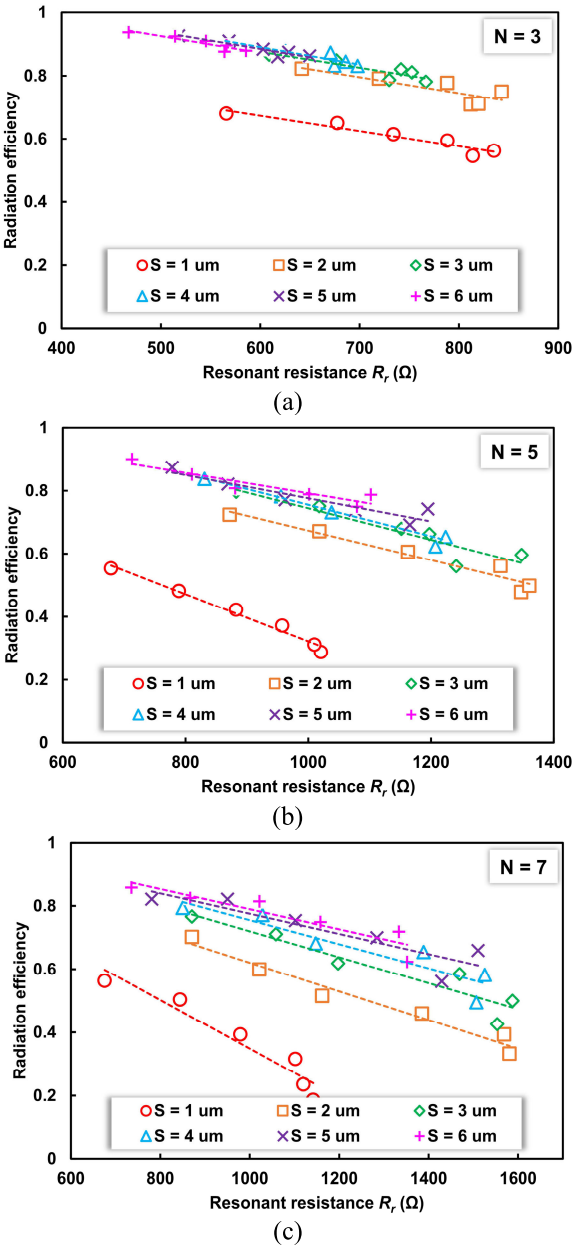


**FIGURE 5.** Radiation efficiency of FDA at 1 THz as a function of resonant resistance in different arm spacing for the case of (a) $N = 3$, (b) $N = 5$, and (c) $N = 7$.

The radiation characteristic of the FDA on semi-infinite Si substrate is displayed in Fig. 6. Most of the electromagnetic wave emitted towards the Si substrate. As the antenna is located on the interface between two media with different permittivity, the radiated power is proportional to $\varepsilon^{3/2}$, where $\varepsilon$ is the substrate to air permittivity ratio. In the virtue of reciprocity theorem, the antenna would receive

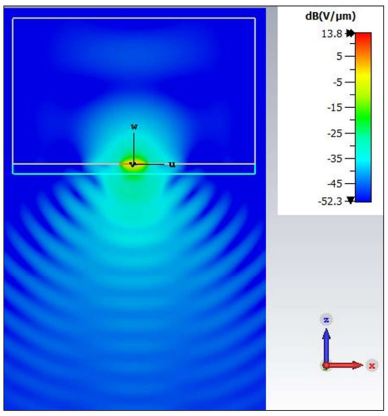


**FIGURE 6.** Electric field radiation characteristic of the semi-infinite substrate thickness shows the majority radiation towards the substrate direction.

power from the substrate-side approximately 40 times larger than that from the airside [21], [22]. The pattern shown in Fig. 6 suggests the effectiveness of the semi-infinite thickness design to eliminate the substrate waves loss during simulation and it is suitable for the initial investigation of the antenna characteristics with efficient computational time [23]. Furthermore, the radiation pattern of all simulated FDA geometries follows the same tendency of substrate side radiation. Hence it can be concluded that the thick Si substrate dominates the radiation pattern rather than the antenna geometry itself.

### B. RECEIVING MODE

In the receiving mode simulation, a heater film was used on the antenna gap replacing the source excitation in the radiating mode. The heater was designed to match the antenna radiation resistance in each geometrical variation extracted in radiating mode simulation. Considering the reciprocity of the design, a 1 V/m radiation source was launched from the substrate side towards z+ direction. Therefore, the uniformly incident power density ($W_i$) can be calculated by

$$W_i = \frac{E^2}{2\eta_s} \tag{3}$$

where $E$ is the electric field intensity of the plane wave and $\eta_s$ is the wave impedance of the substrate material ($\sqrt{\mu/\varepsilon_s} \times \eta_0$). The antenna absorbs the incident power and transfer the energy to the load (heater) causing a power dissipation or loss. The time-average power dissipation ($P_r$) in the heater was numerically calculated based on the integration of the Poynting vectors over the heater surfaces, expressed as

$$P_r = \frac{1}{2}\int_A Re(E \times H^*)dA \tag{4}$$

where $E$ and $H$ is the electric and magnetic field intensity, respectively. Hence from (3) and (4), the power capturing characteristics of the antenna can be calculated as the

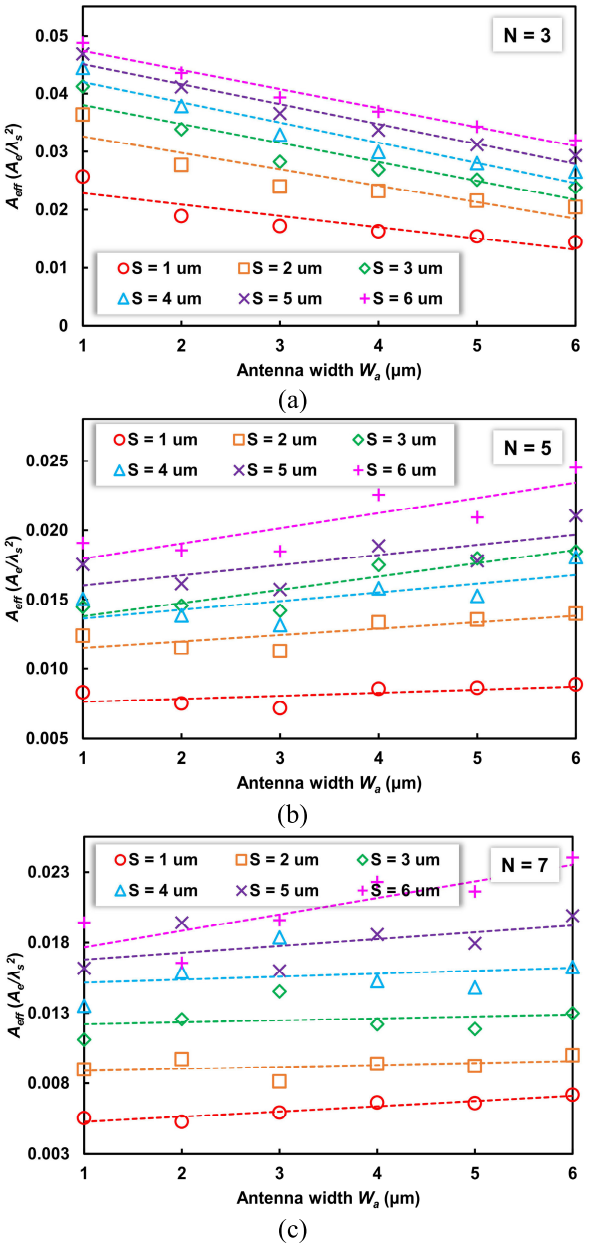


**FIGURE 7.** Antenna area efficiency ($A_{eff}$) as a function of antenna width for different arm spacings for the case of (a) $N = 3$, (b) $N = 5$, and (c) $N = 7$.

effective area ($A_e$) by the following formula,

$$A_e = \frac{P_r}{W_i} \tag{5}$$

where $P_r$ and $W_i$ are represented in Watt and Watt/m$^2$, respectively. Furthermore, the effective area of the receiving antenna was extended to the antenna area efficiency ($A_{eff}$) described as the ratio of the antenna's effective area to its physical area ($A_P$) [24]. Here we regard the diffraction-limited area, i.e. square of the effective wavelength ($\lambda_s^2$) as the $A_P$.

Fig. 7 shows the antenna area efficiency ($A_{eff}$) of FDA as a function of $w_a$ for different $S$ and $N$. The $A_{eff}$ decreases as $N$ increase, which shows similar behavior to the radiation

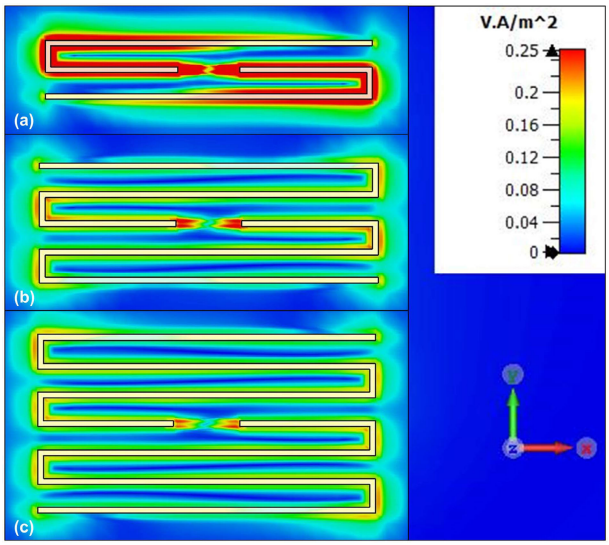


**FIGURE 8.** Power density distribution of folded dipole antenna structures when $w_a = 1$ $\mu$m and $S = 4$ $\mu$m with different number of arms: (a) $N = 3$; (b) $N = 5$; (c) $N = 7$.

efficiency results in Fig. 5 as the effect of higher ohmic loss. However, the $A_{eff}$ results with respect to $w_a$ and $S$ are changed as the number of arms increases. For $N = 3$, the $A_{eff}$ is slightly decrease as the antenna width wider. It shows opposite trend of the radiation efficiency in radiating mode where the narrow width antenna (higher resistance) has lower radiation efficiency. While higher resonant resistance in $N = 5$ and 7 shows a fluctuating $A_{eff}$ to $w_a$. As for arm spacing effect, the $A_{eff}$ increases as the arm spacing becomes wider regardless of the number of arms. The highest $A_{eff}$ of 0.049 is obtained when $N = 3$, $w_a = 1$ $\mu$m and $S = 6$ $\mu$m. Compared to the FDA with number of arms of 5 and 7, three-arm FDA has an obvious advantage in that it provides higher peak area efficiency. Furthermore, its simpler structure is beneficial in terms of device fabrication.

Fig. 8 shows the power density distribution in the FDA surface for $w_a = 1$ $\mu$m and $S = 4$ $\mu$m. The energy is distributed on the antenna line and gap area. As $N$ increases, the average induced energy decreases due to larger antenna surface area. This means the total energy density on the antenna structure is higher compared to the one absorbed into heater. Typically, the power loss on antenna surface does not contribute to the overall antenna-coupled bolometer performance, since only the heater part is fabricated in suspended structure above cavity hole. Hence the temperature increase in the bolometer mainly depends on the heater power loss rather than power loss in the antenna surface.

## IV. DISCUSSION

The area efficiency of FDA is relatively lower with the maxima close to 5 percent according to Fig. 7. However, the responsivity improvement could also be expected from the higher electrical resistance, even with low area efficiency caused by high conduction loss from the antenna surface. The bolometer responsivity is defined as the ratio of electrical

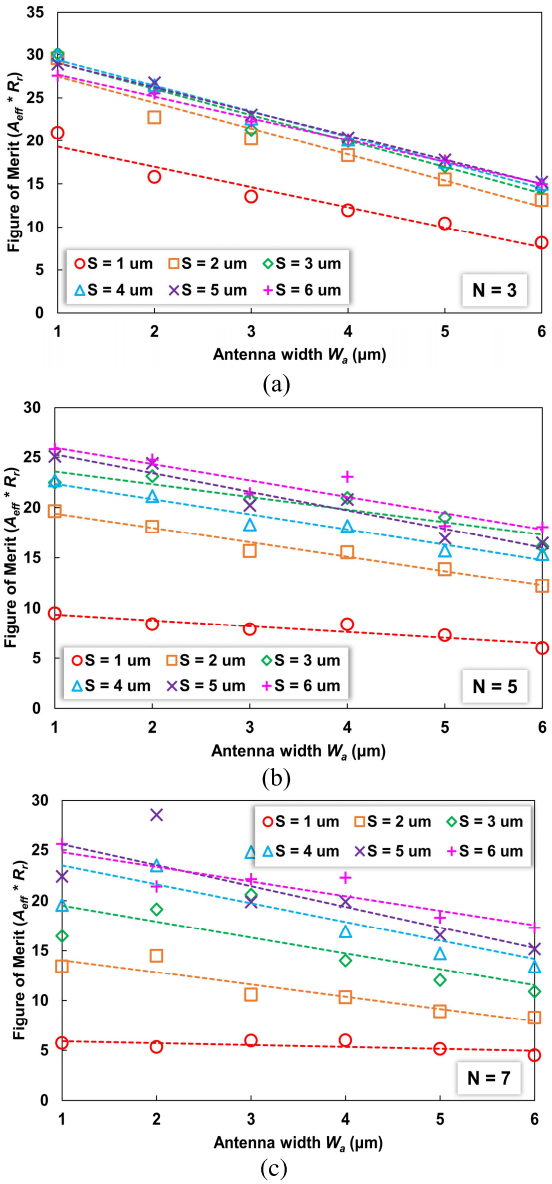


**FIGURE 9.** Figure of merit (FOM) as a function of antenna width for different arm spacings for the case of (a) $N = 3$, (b) $N = 5$, and (c) $N = 7$.

output signal of the bolometer to the input radiation power from the source, with the unit of volts per watt (V/W) or amperes per watt (A/W) if the output signal current is measured. When a THz radiation incident upon bolometer surface, the power is absorbed and cause a temperature increase. According to the heat transfer equation, the output signal voltage ($V_s$) measured in the bolometer is proportional to [25]

$$V_s \propto \frac{\alpha A_D P_o}{G} \tag{6}$$

where $\alpha$ is the temperature coefficient of resistance (TCR) of the bolometer material, $A_D$ is the detector area, $P_o$ is the incident radiation power density, and $G$ is the effective thermal conductance of the bolometer. In the presence of an

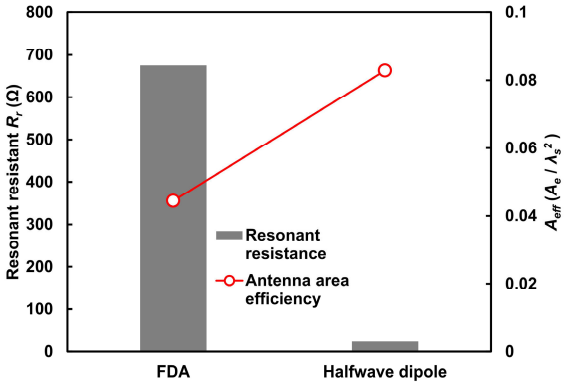


**FIGURE 10.** Resonant resistance and antenna area efficiency comparison between FDA and half-wave dipole antenna.

antenna as an absorbing component, the detector area could be replaced by the effective area ($A_e$) of the antenna. Antenna with a large effective area is preferable to absorb and transfer more power to the bolometer hence increase the output signal, as long as both impedances are closed to each other. The other way to increase the responsivity is by reducing the overall thermal conductance of the bolometer by downscaling it. A smaller bolometer leads to larger thermal resistance that is correlated to the electrical resistance $R_h$ of the heater. Consequently, the antenna should sufficiently enhance its resistance for the proper impedance matching between the two. However, the typical high impedance antenna has lower efficiency due to high ohmic losses in the antenna surfaces. Therefore, to consider the trade-off between antenna efficiency and resistance, we use the product of the antenna area efficiency and heater resistance as the figure of merit (FOM) to evaluate the overall bolometer performance improvement made by the FDA,

$$FOM = A_{eff} \times R_h \tag{7}$$

With this definition, a higher FOM is preferable since it corresponds to the responsivity improvement of the antenna-coupled bolometer.

Fig. 9 shows the FOM of various FDA geometries calculated from (7). Please remember that the heater resistance ($R_h$) was set equal to the resonant resistance ($R_r$) of the antenna based on simulation in radiating mode. It is clear that three-arm FDA has higher FOM compared to the 5- and 7-arm FDA. The optimum FOM is 30 in when N = 3, for 1-$\mu$m wide and 4-$\mu$m arm spacing. FDA with number of arms larger than 3 shows rather stable FOM but with slight effect to the antenna width. The FOM is increasing with the arm spacing and shows higher saturation point as the number of arms increase. These results reveal that the antenna-coupled bolometer could be improved with the folded dipole antenna and high resistance heater. However, the trade-off between resistance and antenna efficiency must be considered in order to find the optimum condition.

To justify the responsivity improvement being made by high impedance antenna and heater, a comparison with half-wave dipole antenna was made. We designed a half-wave dipole antenna with 45-$\mu$m long, 3-$\mu$m wide, and simulated it with the setup. A resonant resistance ($R_r$) of 23Ω was obtained at 1 THz with the area efficiency of 0.083 from radiating and receiving mode simulations. Fig. 10 shows the $R_r$ and $A_{eff}$ comparison between FDA and half-wave dipole antenna which reveals the FOM improvement by a factor of 15 can be expected by the implementation of FDA. However, the improvement factor could be different if the comparison is made with different type of antenna used for antenna-coupled detectors, such as bowtie, spiral and log-periodic antennas with various efficiency, impedance and bandwidth. In this report, we intended to see the performance improvement in the wide range of the heater resistance, and thus the FDA is chosen among many types of antennas since it can realize variety of resonant resistance by changing number of arms, arm spacing and width. A comparison with the half-wave dipole antenna is made because it is a typical planar antenna for antenna-coupled microbolometer.

## V. CONCLUSION

In this paper, we designed and electromagnetically simulated the folded dipole antennas (FDA) with various dimensions for 1-THz operation. FDA was selected to realize high input impedance required for improving the performance of the antenna-coupled bolometer with high-resistance heater. Structural design and simulation results were presented in radiating and receiving modes to study the impact of different structural parameters of the FDA on input impedance and area efficiency, respectively. The higher number of arms and longer effective length of FDA contributed to the increase of input impedance and decrease of antenna area efficiency. We proposed that that the bolometer responsivity could be predicted by the product of antenna area efficiency and resonant resistance. Simulation in various FDA geometries was performed, and the optimum performance was obtained by the three-arm FDA with 1-$\mu$m antenna width and 4-$\mu$m arm spacing. A comparison with half-wave dipole antenna with low impedance heater showed that the bolometer responsivity could be enhanced by a factor of 15. This research could be regarded as the first step in demonstrating the feasibility of high-impedance antenna for the antenna-coupled THz bolometer. Moreover, the proposed method could also provide the design procedure of the antenna for THz detector applications such as imaging for non-destructive inspection.

## ACKNOWLEDGMENT

The authors are grateful to Prof. Erik Bründermann of the Karlsruhe Institute of Technology and Emeritus Prof. Norihisa Hiromoto of Shizuoka University for fruitful discussions and kind guidance.

## REFERENCES


[1] S. S. Dhillon, "The 2017 terahertz science and technology roadmap," *J. Phys. D, Appl. Phys.*, vol. 50, no. 4, Feb. 2017, Art. no. 043001, doi: 10.1088/1361-6463/50/4/043001.

[2] G. Valušis, A. Lisauskas, H. Yuan, W. Knap, and H. G. Roskos, "Roadmap of terahertz imaging 2021," *Sensors*, vol. 21, no. 12, p. 4092, Jun. 2021, doi: 10.3390/s21124092.

[3] A. Gong, Y. Qiu, X. Chen, Z. Zhao, L. Xia, and Y. Shao, "Biomedical applications of terahertz technology," *Appl. Spectrosc. Rev.*, vol. 55, no. 5, pp. 418–438, May 2020, doi: 10.1080/05704928.2019.1670202.

[4] K. Wang, D.-W. Sun, and H. Pu, "Emerging non-destructive terahertz spectroscopic imaging technique: Principle and applications in the agri-food industry," *Trends Food Sci. Technol.*, vol. 67, pp. 93–105, Sep. 2017, doi: 10.1016/j.tifs.2017.06.001.

[5] C. Risacher, R. Gusten, J. Stutzki, H.-W. Hubers, D. Buchel, U. U. Graf, S. Heyminck, C. E. Honingh, K. Jacobs, B. Klein, T. Klein, C. Leinz, P. Putz, N. Reyes, O. Ricken, H.-J. Wunsch, P. Fusco, and S. Rosner, "First supra-THz heterodyne array receivers for astronomy with the SOFIA observatory," *IEEE Trans. THz Sci. Technol.*, vol. 6, no. 2, pp. 199–211, Mar. 2016, doi: 10.1109/TTHZ.2015.2508005.

[6] J. F. O'Hara, S. Ekin, W. Choi, and I. Song, "A perspective on terahertz next-generation wireless communications," *Technologies*, vol. 7, no. 2, p. 43, Jun. 2019, doi: 10.3390/technologies7020043.

[7] A. Rogalski, *Infrared and Terahertz Detectors*, 3rd ed. Boca Raton, FL, USA: CRC Press, 2019.

[8] M. Aoki, M. Takeda, and N. Hiromoto, "Electromagnetic simulation for THz antenna-coupled microbolometers operated at room temperature," *MAKARA J. Technol. Ser.*, vol. 17, no. 1, pp. 1–6, Sep. 2013, doi: 10.7454/mst.v17i1.1919.

[9] P. L. Richards, "Bolometers for infrared and millimeter waves," *J. Appl. Phys.*, vol. 76, no. 1, pp. 1–24, Aug. 1994, doi: 10.1063/1.357128.

[10] A. Banerjee, H. Satoh, D. Elamaran, Y. Sharma, N. Hiromoto, and H. Inokawa, "Performance improvement of on-chip integrable terahertz microbolometer arrays using nanoscale meander titanium thermistor," *J. Appl. Phys.*, vol. 125, no. 21, Jun. 2019, Art. no. 214502, doi: 10.1063/1.5083643.

[11] T. Endo, Y. Sunahara, S. Satoh, and T. Katagi, "Resonant frequency and radiation efficiency of meander line antennas," *Electron. Commun. Jpn. II, Electron.*, vol. 83, no. 1, pp. 52–58, Jan. 2000, doi: 10.1002/(SICI)1520-6432(200001)83:1<52:AID-ECJB7>3.0.CO.2-7.

[12] H.-C. Ryu, "Folded dipole antenna for power enhancement of a terahertz photomixer," *J. Korean Phys. Soc.*, vol. 64, no. 10, pp. 1556–1560, May 2014, doi: 10.3938/jkps.64.1556.

[13] L. Liu, S. M. Rahman, Z. Jiang, W. Li, and P. Fay, "Advanced terahertz sensing and imaging systems based on integrated III–V interband tunneling devices," *Proc. IEEE*, vol. 105, no. 6, pp. 1020–1034, Jun. 2017, doi: 10.1109/JPROC.2016.2636245.

[14] J. Montero-de-Paz, E. Ugarte-Munoz, L. E. Garcia-Munoz, I. Camara Mayorga, and D. Segovia-Vargas, "Meander dipole antenna to increase CW THz photomixing emitted power," *IEEE Trans. Antennas Propag.*, vol. 62, no. 9, pp. 4868–4872, Sep. 2014, doi: 10.1109/TAP.2014.2346708.

[15] W. Yin, S. K. Khamas, and R. A. Hogg, "High input resistance terahertz dipole antenna with an isolating photonic band gap layer," in *Proc. 10th Eur. Conf. Antennas Propag. (EuCAP)*, Apr. 2016, pp. 1–3, doi: 10.1109/EuCAP.2016.7481333.

[16] N. Llombart and A. Neto, "THz time-domain sensing: The antenna dispersion problem and a possible solution," *IEEE Trans. THz Sci. Technol.*, vol. 2, no. 4, pp. 416–423, Jul. 2012, doi: 10.1109/TTHZ.2012.2197949.

[17] T. K. Nguyen and I. Park, "Resonant antennas on semi-infinite and lens substrates at terahertz frequency," in *Convergence of Terahertz Sciences in Biomedical Systems*. Dordrecht, The Netherlands: Springer, 2012, pp. 181–193, doi: 10.1007/978-94-007-3965-9_9.

[18] T. Weiland, M. Timm, and I. Munteanu, "A practical guide to 3-D simulation," *IEEE Microw. Mag.*, vol. 9, no. 6, pp. 62–75, Dec. 2008, doi: 10.1109/MMM.2008.929772.

[19] W. M. Haynes, D. R. Lide, and T. J. Bruno, *CRC Handbook of Chemistry and Physics*, 97th ed. Boca Raton, FL, USA: CRC Press, 2016.

[20] A. Banerjee, H. Satoh, A. Tiwari, C. Apriono, E. T. Rahardjo, N. Hiromoto, and H. Inokawa, "Width dependence of platinum and titanium thermistor characteristics for application in room-temperature antenna-coupled terahertz microbolometer," *Jpn. J. Appl. Phys.*, vol. 56, no. 4S, Apr. 2017, Art. no. 04CC07, doi: 10.7567/JJAP.56.04CC07.

[21] B. A. Lail, C. T. Middlebrook, P. M. Krenz, and G. D. Boreman, "Infrared dipole-coupled bolometer response on a hemispherical silicon immersion lens," *Infr. Phys. Technol.*, vol. 52, nos. 2–3, pp. 89–96, Mar. 2009, doi: 10.1016/j.infrared.2009.03.001.

[22] J. Alda, C. Fumeaux, M. A. Gritz, D. Spencer, and G. D. Boreman, "Responsivity of infrared antenna-coupled microbolometers for air-side and substrate-side illumination," *Infr. Phys. Technol.*, vol. 41, no. 1, pp. 1–9, Feb. 2000, doi: 10.1016/S1350-4495(99)00036-5.

[23] T. K. Nguyen and I. Park, "Comparative study of stripline dipole antenna on semiinfinite and lens substrates at terahertz frequency," in *Proc. 8th Eur. Conf. Antennas Propag. (EuCAP)*, Apr. 2014, pp. 2470–2474, doi: 10.1109/EuCAP.2014.6902319.

[24] T. Morf, "Wide bandwidth room-temperature THz imaging array based on antenna-coupled MOSFET bolometer," *Sens. Actuators A, Phys.*, vol. 215, pp. 96–104, Aug. 2014, doi: 10.1016/j.sna.2014.03.019.

[25] P. W. Kruse, *Uncooled Thermal Imaging Arrays, Systems, and Applications*. Bellingham, WA, USA: SPIE, 2001.


**ARIE PANGESTI AJI** was born in Bandung, Indonesia, in 1987. He received the Bachelor of Applied Science (B.A.Sc.) degree in telecommunication engineering from Politeknik Elektronika Negeri Surabaya, in 2009, the Master of Engineering (M.E.) degree in electrical engineering from Universitas Indonesia, in 2018, and the Doctor of Philosophy in Engineering (Ph.D.) degree in nanovision technology from Shizuoka University, in 2022. He is currently pursuing the Ph.D. degree with Universitas Indonesia under the Double-Degree Program.

His research interests include terahertz engineering, antenna design and optimization, and microwave technology.

**HIROAKI SATOH** (Member, IEEE) received the B.E. degree from Muroran Institute of Technology, Hokkaido, Japan, in 1999, and the M.E. and Ph.D. degrees from Hokkaido University, Hokkaido, in 2001 and 2004, respectively.

He was a Research Associate with the University of Tokushima, Tokushima, Japan, from 2004 to 2007. Since 2007, he has been an Assistant Professor with the Research Institute of Electronics, Shizuoka University, Hamamatsu. His current research interest includes computational electromagnetics and its application to silicon nanodevices for advanced photonics.

Dr. Satoh is a member of the Japan Society of Applied Physics, the Institute of Electronics, Information and Communication Engineers, Japan, and the Institute of Electrical Engineers of Japan.

**CATUR APRIONO** (Member, IEEE) received the B.Eng. and M.Eng. degrees in telecommunication engineering from the Department of Electrical Engineering, Universitas Indonesia, Indonesia, in 2009 and 2011, respectively, and the Ph.D. degree in nanovision technology from Shizuoka University, Japan, in 2015.

Since 2018, he has been an Assistant Professor of telecommunication engineering with Universitas Indonesia, where he is currently a Lecturer with the Department of Electrical Engineering, Faculty of Engineering. His main research interests include antenna and microwave engineering, terahertz wave technology, and optical communications. He has been a member of the IEEE Antenna and Propagation Society (AP-S) and the IEEE Microwave Theory and Technique Society (MTT-S). He has involvement in the IEEE Joint Chapter MTT/AP Indonesia Section, as a Secretary and a Treasurer, in 2017, 2018, and 2019, and active in various chapter activities, such as the First Indonesia–Japan Workshop on Antennas and Wireless Technology (IJAWT), as a Secretary, and the 2019 IEEE International Conference on Antenna Measurements Applications (CAMA), Bali, in October 2019, as a Treasurer.

**EKO TJIPTO RAHARDJO** (Member, IEEE) was born in Pati, Indonesia, in 1958. He received the Ir. degree in electrical engineering from Universitas Indonesia, Depok, Indonesia, in 1981, the M.S. degree in electrical engineering from the University of Hawai'i at Mānoa, Honolulu, HI, USA, in 1987, and the Ph.D. degree in electrical engineering from Saitama University, Urawa, Japan, in 1996.

Since 1982, he has been a Teaching Assistant with the Department of Electrical Engineering, Universitas Indonesia. From 1997 to 2004, he was the Head of the Telecommunication Laboratory, Department of Electrical Engineering, Universitas Indonesia, where he was the Executive Director of the Quality Undergraduate Education (QUE), from 1999 to 2004. Since 2003, he has been the Director of the Antenna Propagation and Microwave Research Group (AMRG), Universitas Indonesia. He was the Head of the Department of Electrical Engineering, Universitas Indonesia, from 2004 to 2008. Since 2005, he has been a Professor of electrical engineering. He was the Chairperson of the University Senate, Universitas Indonesia, from 2011 to 2012. He has published and presented more than 100 research articles in national and international journals and symposiums. His research interests include antenna engineering, wave propagation, microwave circuits, communication systems, and telecommunications system regulation.

Prof. Rahardjo is a member of the IEEE Antenna and Propagation Society (AP-S) and the IEEE Microwave Theory and Technique Society (MTTS). He has been a member of the International Steering Committee (ISC) of the Asia–Pacific Microwave Conference (APMC), since 2010, and the International Advisory Board of the International Symposium on Antenna and Propagation (ISAP), since 2012. He received the Indonesian Government Scholarship through MUCIA, from 1984 to 1987, the Hitachi Scholarship, from 1992 to 1996, the Young Researcher's Award from Universitas Indonesia, in 1996, the second winner of the Best Researcher Award in Science and Technology from Universitas Indonesia, in 2009, and the second winner of the Best Teaching Award from Universitas Indonesia, in 2010. He was the General Chairperson of the Indonesia–Malaysia Microwave and Antenna Conference (IMMAC), Depok, in 2010, and the Indonesia–Japan Joint Scientific Symposium (IJJSS), Bali, in 2010, and the General Co-Chairperson of IJJSS, Chiba, Japan, in 2012. In addition, he was the General Chair of the 1st Indonesia–Japan Workshop on Antennas and Wireless Technology (IJAWT), Depok, in 2017, and the 2019 IEEE International Conference on Antenna Measurements and Applications (CAMA), Bali, in October 2019. He was the Founder of the IEEE Joint Chapter MTTS/AP-S, Indonesia. He has served as the President for the IEEE Joint Chapter MTT-S/AP-S, from 2009 to 2010, and the IEEE Indonesia Section, from 2014 to 2015.

**HIROSHI INOKAWA** (Member, IEEE) received the Ph.D. degree in electrical engineering from Kyoto University, Kyoto, Japan, in 1985.

In 1985, he joined Atsugi Electrical Communications Laboratories, Nippon Telegraph and Telephone Corporation (NTT), Kanagawa, Japan. Since then, he has been engaged in the research and development of scaled-down CMOS devices and silicon single-electron devices. He was a Researcher with the National Institute of Science and Technology Policy (NISTEP), from 2002 to 2018. In 2006, he became a Professor with the Research Institute of Electronics, Shizuoka University, Hamamatsu, Japan, where he has been studying nanodevices for advanced circuits and systems. He is a member of the Japan Society of Applied Physics (JSAP), the Institute of Electronics, Information and Communication Engineers of Japan (IEICE), and the Institute of Electrical Engineers of Japan (IEEJ). He has served as a JSAP Board Member (Representative), from 2001 to 2003, an Editor for *JJAP*, from 2007 to 2013, and the Chair for the IEEJ Survey Committee of Silicon Nanosystem Integration Technology, from 2009 to 2011.